View metadata, citation and similar papers at core.ac.uk
brought to you by CORE
provided by Apollo

Complementary spin-Hall and inverse spin-galvanic effect torques in a ferromagnet/semiconductor bilayer

T. D. Skinner,[1, a)] K. Olejník,[2] L. K. Cunningham,[1] H. Kurebayashi,[1, 3, b)] R. P. Campion,[4] B. L. Gallagher,[4] T. Jungwirth,[2, 4] and A. J. Ferguson[1, c)]

[1)] *Cavendish Laboratory, University of Cambridge, CB3 0HE, United Kingdom*

[2)] *Institute of Physics, ASCR, v.v.i., Cukrovarnicka 10, 16253 Praha 6, Czech Republic*

[3)] *PRESTO, Japan Science and Technology Agency, Kawaguchi 332-0012, Japan*

[4)] *School of Physics and Astronomy, University of Nottingham, Nottingham NG7 2RD, United Kingdom*

(Dated: 30 January 2015)

[a)] email: timothy.skinner@ucl.ac.uk; Present address: London Centre for Nanotechnology, University College London, WC1H 0AH, United Kingdom

[b)] Present address: London Centre for Nanotechnology, University College London, WC1H 0AH, United Kingdom

[c)] email: ajf1006@cam.ac.uk

Recently discovered relativistic spin torques induced by a lateral current at a ferromagnet/paramagnet interface are a candidate spintronic technology for a new generation of electrically-controlled magnetic memory devices. The focus of our work is to experimentally disentangle the perceived two model physical mechanisms of the relativistic spin torques, one driven by the spin Hall effect and the other one by the inverse spin galvanic effect. To achieve this we prepared an epitaxial transition-metal-ferromagnet/semiconductor-paramagnet single-crystal structure and performed a room-temperature vector analysis of the torques by means of the all-electrical ferromagnetic resonance technique. By choice of our structure in which the semiconductor-paramagnet has a Dresselhaus crystal inversion-asymmetry, the system is favourable for separating the torques due to the inverse spin galvanic effect and spin Hall effect mechanisms into the field-like and antidamping-like components, respectively. Since they contribute to distinct symmetry torque components, the two microscopic mechanisms do not compete but complement each other in our system.

Introduction

The two considered microscopic origins of the relativistic spin torques observed at a ferromagnet/paramagnet interface[1,2] have the following basic characteristics: In one picture, a spin-current generated in the paramagnet via the relativistic spin Hall effect[3] (SHE) is absorbed in the ferromagnet and induces the spin transfer torque[4] (STT). In the other picture, a non-equilibrium spin-density is generated via the relativistic inverse spin galvanic effect[5] (ISGE) and induces the spin-orbit torque[6–8] (SOT) in the ferromagnet. From the early observations in paramagnetic semiconductors, SHE and ISGE are known as companion phenomena that can both allow for electrically aligning spins in the same structure[9–11]. It is therefore both challenging and desirable for our basic physical understanding of the spin torques at the ferromagnet/paramagnet interface to experimentally disentangle the SHE and ISGE contributions.

The splitting of the two microscopic mechanisms between the field-like and the antidamping-like torque components has not been previously achieved for several conceptual reasons. The original theoretical proposals[12–14] and experimental observations[10,11,15,16] of the ISGE were

made in paramagnets with no ferromagnetic component in the structure. The corresponding non-equilibrium spin-density, generated in the ISGE by inversion-asymmetry terms in the relativistic Hamiltonian, has naturally no dependence on magnetization. Hence, in the context of magnetic semiconductors[6,8,17,18] or ferromagnet/paramagnet structures[1,7,19–21], the ISGE may be expected to yield only the field-like component of the torque $\sim \mathbf{M} \times \boldsymbol{\zeta}$, where the vector $\boldsymbol{\zeta}$ is independent of the magnetization vector $\mathbf{M}$ (see Fig. 1a). However, when carriers experience both the spin-orbit coupling and magnetic exchange coupling, the inversion asymmetry can generate a non-equilibrium spin density component of extrinsic, scattering-related[22,23] or intrinsic, Berry-curvature[24–26] origin which is magnetization dependent and yields an antidamping-like torque $\sim \mathbf{M} \times (\mathbf{M} \times \boldsymbol{\zeta})$. Experiments in (Ga,Mn)As confirmed the presence of the ISGE-based mechanism[8,17,18] and demonstrated that the field-like and the Berry-curvature antidamping-like SOT components can have comparable magnitudes[25].

The STT is dominated by the antidamping-like component[4] in weakly spin-orbit coupled ferromagnets with $\tau_{\text{ex}} \ll \tau_s$, where τ_{ex} is the precession time of the carrier spins in the exchange field of the ferromagnet and τ_s is the spin life-time in the ferromagnet. This, in principle, applies also to the case when the spin current is injected to the ferromagnet from a paramagnet via the SHE (see Fig. 1b). However, at finite τ_{s}, the STT also acquires a field-like component[4]. Experiments in W/Hf/CoFeB structures confirmed the presence of the SHE-based mechanism in the observed torques and showed that the SHE-STT can have both antidamping-like and field-like components of comparable magnitudes[27].

In the commonly studied polycrystalline transition-metal-ferromagnet/heavy-metal-paramagnet samples, the dependence of the torques on the angle of the driving in-plane current also does not provide the direct means to disentangle the two microscopic origins. The lowest order inversion-asymmetry spin-orbit terms in the Hamiltonian have the Rashba form (see Fig. 1d) for which the vector $\boldsymbol{\zeta}$ is in the plane parallel to the interface and perpendicular to the current, independent of the current direction. The same applies to the spin-polarization of the SHE spin-current propagating from the paramagnet to the ferromagnet. The $\mathbf{M}$ and $\boldsymbol{\zeta}$ functional form of the field-like and antidamping-like SHE-STTs is the same as of the corresponding SOT components. In the observed lowest order torque terms in Pt/Co and Ta/CoFeB structures[28] the ISGE-based and the SHE-based mechanism remained, therefore, indistinguishable. The simultaneous observation of higher order torque terms in these sam-

ples pointed to SOTs due to structural inversion-asymmetry terms beyond the basic Rashba model. From the Ta thickness dependence measurements in the Ta/CoFeB structure it was concluded that in these samples both the ISGE-based and the SHE-based mechanisms contributed to both the field-like and the antidamping-like torques[29] .

The SHE and ISGE were originally discovered in III-V semiconductors[9–11,15,16] but for maximizing the relativistic spin torques in common transition-metal ferromagnets it turned out to be more suitable to interface them with the highly conductive heavy-metal paramagnets like Pt, Ta, or W[1,2,27–29]. Rather than enhancing the magnitude of the torques, the aim of our study is to clearly separate the two microscopic origins for which returning to the III-V semiconductor paramagnets is instrumental. In experiments presented below we succeed to disentangle the torques into the ISGE driven field-like component and the SHE driven antidamping-like component using a 2 nm thick single crystal Fe grown epitaxially without breaking vacuum on top of a 20 nm thick p-doped GaAs epilayer (see Methods).

Among the inversion-asymmetry terms characteristic of our system, the Rashba term due to the structural asymmetry of the bilayer plays a minor role. Instead, the leading role is played by the broken inversion symmetry in the crystal structure of the semiconductor paramagnet. Independent of the interface, holes in the strained zinc-blende lattice of the III-V semiconductor experience a linear-in-wavevector Dresselhaus spin-orbit coupling. The ISGE of the corresponding symmetry (see Fig. 1c) generated in the semiconductor induces the SOT in the adjacent Fe film with $\boldsymbol{\zeta}$ perpendicular to the current for current along [110] or [1$\bar{1}$0] crystal axes of the semiconductor, while $\boldsymbol{\zeta}$ is parallel to the current for the [100] or [010] current directions. Moreover, the ISGE with this characteristic Dresselhaus symmetry generated in the semiconductor paramagnet induces only the field-like torque in the adjacent Fe while the antidamping-like SOT component with this symmetry is absent by design as the ferromagnetic moments of the Fe are spatially separated from the bulk-inversion asymmetry of the semiconductor-paramagnet. Additionally, the SHE spin-current can be readily generated inside the paramagnetic p-doped GaAs layer and absorbed in the weakly spin-orbit coupled Fe in the form of the antidamping-like STT.

To obtain measurable torques in a metal-ferromagnet/semiconductor-paramagnet structure requires at least partially matched conductances of the semiconductor and metal layers which

we achieved by doping the GaAs host with $\sim 3\%$ of substitutional Mn_{Ga} acceptors. Mn allows us to achieve this exceptionally high charge-doping. Simultaneously, at 3% Mn, hole bands within the (Ga,Mn)As semiconductor do not experience a sizeable enough magnetic exchange splitting at room temperature that would generate an observable Dresselhaus-symmetry antidamping-like SOT in our structure.

In the following, we measure the relativistic spin torques in the Fe/(Ga,Mn)As bilayer using an electrically induced and detected FMR technique[18,30]. From magnetisation angle dependence measurements of the FMR voltages we find the field-like and anti-damping torques have similar magnitudes. By measuring devices where the current is along different crystal directions of the semiconductor, we show that the symmetry of the field-like torque is dominated by a Dresselhaus term, whereas the anti-damping torque is independent of the crystal direction. These symmetries show us that the field-like torque can be ascribed to the SOT and the anti-damping torque to the STT.

Results

Electrically-induced FMR measurements

Current-induced torques were measured in 10×200 μm patterned bars using an all-electrical FMR technique (see Fig. 2a). In this method, a microwave current flowing in the device induces FMR when the externally applied magnetic field matches the resonant condition. The resonance of the Fe magnetisation is detected in the dc voltage induced across the bar, $V_{\rm dc}$. This is due to the homodyne mixing of the microwave current with the oscillating component of magnetoresistance caused by the magnetisation precession. In these measurements we increase the microwave current coupled into the sample, with a typical resistance of 8 kΩ, by using an impedance matching network[30] (see Methods and supplementary note 1).

For a series of external magnetic field directions in the plane of the sample, FMR sweeps were recorded using a microwave frequency of close to 16 GHz. From the magnetisation angle-dependence of the resonance field, we obtained the magnetisation amplitude value of $\mu_0 M_{\rm s} = 1.85 \pm 0.03$ T which is close to the literature value of 1.7 T for Fe[31], and we found an in-plane uniaxial anisotropy of $\mu_0 {\rm H_U} = 0.101 \pm 0.001$ T which is typical for thin films of Fe grown on GaAs[32]. By solving the Landau-Lifshitz-Gilbert equation for a small current

induced excitation field, $(h_\mathrm{x}, h_\mathrm{y}, h_\mathrm{z})e^{j\omega t}$, V_dc is found to be comprised of symmetric and antisymmetric Lorentzian functions with coefficients V_sym and V_asy respectively. Here h_x is the excitation field component parallel to the current and h_y is the component perpendicular to the current. h_z is the component perpendicular to the plane of the bilayer. The coefficients depend on the angle, θ, of the magnetisation vector relative to the current and are given by

$$\begin{aligned} V_\mathrm{sym} &= V_\mathrm{mix} A_\mathrm{yz} \sin 2\theta h_\mathrm{z}, \\ V_\mathrm{asy} &= V_\mathrm{mix} A_\mathrm{yy} \sin 2\theta (h_\mathrm{y} \cos\theta - h_\mathrm{x} \sin\theta). \end{aligned} \tag{1}$$

Here, V_mix is the sensitivity of the mixing detection and is given by $V_\mathrm{mix} = -\frac{1}{2} I_0 \Delta R$, where I_0 $(e^{j\omega t}, 0, 0)$ is the microwave current in the device and ΔR is the coefficient of the anisotropic magnetoresistance of the sample. A_yy and A_yz are the diagonal and off-diagonal components of the ac magnetic susceptibility, which depend on the magnetic anisotropies and Gilbert damping of the sample. In our devices, ΔR is typically 17 Ω which, assuming Fe carries the majority of the current in the bilayer, is consistent in sign and magnitude with literature values of 0.2% anisotropic magnetoresistance in Fe.[33] We estimate the proportion of total bilayer current in the Fe layer to be 79% by resistance measurements of Hall bars before and after removing the Fe and capping Al (see supplementary note 2).

FMR measurements were made using devices patterned in four crystal directions. The microwave power for all devices, incident on the impedance matching network, was 24 dBm. For each angle, the resonances were fitted by symmetric and antisymmetric Lorentzian functions. A typical curve is shown in Fig. 2b. The in-plane uniaxial magnetic anisotropy of Fe implies that, in general, the magnetisation does not lie along the external field. The actual magnetisation angles and uniaxial anisotropy are self-consistently calculated from the dependence of the resonant field on the external magnetic field angle[34]. This also allows the susceptibilities, A_yz and A_yy, to be calculated. The magnetisation angle dependence of $V_\mathrm{sym}/A_\mathrm{yz}$ and $V_\mathrm{asy}/A_\mathrm{yy}$ is plotted in Fig. 2c for a bar patterned in the [010] crystal direction.

Validity of FMR analysis

Our analysis of the current-induced torques using equation (1) is not necessarily valid if the torques do not act in phase with the microwave current. In comparison to electrically detected FMR measurements where the microwave current is capacitively or inductively

coupled into the sample[35], we do not expect a phase-shift between the microwave current and induced fields as the current is conducted ohmically. Nevertheless, we might worry that some part of our microwave resonator circuit leads to a phase shift. To test this, we repeated our measurements with a [100] device over a frequency range (11.8 to 14.4 GHz) using a microstrip resonator with a fundamental frequency close to 13 GHz (Fig. 3a). If there were some frequency dependent phase shift, we would expect the lineshape to oscillate between an antisymmetric and symmetric Lorentzian over this frequency range. However, the ratio of V_{sym} to V_{asy} remains constant in this frequency range to within experimental error (Fig. 3b), confirming that our analysis is correct.

Analysis of the current-induced torques

As shown in Fig. 4a, the in-plane current-induced field depends strongly on the crystal direction of the current and can be well fitted by the Dresselhaus-symmetry ISGE field, $\mathbf{h}^{\mathrm{ISGE}} \sim \left(\cos 2\phi_{[100]}, -\sin 2\phi_{[100]}, 0\right)$, where $\phi_{[100]}$ is the angle between the current and the [100] crystal direction. This is the expected symmetry of the current-induced non-equilibrium spin-polarisation of carriers in the semiconductor due to the inversion-asymmetric crystal structure of the strained zinc-blende lattice of (Ga,Mn)As. The interface exchange coupling of these polarized carriers with the adjacent Fe moments induces the field-like SOT in Fe with the Dresselhaus symmetry. We note that other torque terms with the symmetry common to the Rashba ISGE, the field-like component of the SHE-STT, or the torque due to an Oersted field have only a minor contribution to the total measured field-like torque.

To highlight that carriers in the semiconductor layer are responsible for the Dresselhaus-symmetry ISGE field, we compare Fig. 4a with previous measurements in which the in-plane current induced fields were measured in a bare (Ga,Mn)As epilayer[25] without the Fe film. To observe the corresponding SOT in this sample, a larger concentration of magnetic Mn-moments was used, and the measurements were performed at low temperatures where the Mn moments are ferromagnetic in equilibrium. Instead of the interfacial exchange coupling to Fe, the current induced non-equilibrium spin-polarisation of carriers in the semiconductor due to the Dresselhaus-symmetry ISGE is exchange-coupled directly to the ferromagnetic moments on which it exerts the field-like SOT. In both the Fe/(Ga,Mn)As and the

(Ga,Mn)As samples the same crystal-symmetry field-like SOT is observed which confirms their common Dresselhaus ISGE origin.

In contrast to the in-plane field, the out-of-plane current induced field is independent of the crystal direction of the current but depends on the magnetisation angle. It is dominated by a term $\mathbf{h}^{\mathrm{SHE}} \sim \mathbf{M} \times \mathbf{y}$ ($\mathbf{y}$ is the direction perpendicular to the current) which generates the antidamping-like torque. As shown in Fig. 4b, the amplitudes of the field-like and antidamping-like torques are comparable in our Fe/(Ga,Mn)As structure. The underlying microscopic mechanism of the antidamping-component can only be of the SHE-STT origin. The experimental error shown in Fig. 4b is greater than any crystal dependent variation in the spin-Hall angle.

In previous measurements in the bare (Ga,Mn)As epilayer,[25] the antidamping-like SOT was dominated by the counterpart microscopic mechanism to the Dresselhaus ISGE. This Dresselhaus-symmetry antidamping-like SOT is clearly missing in our measured data. It is suppressed in our Fe/(Ga,Mn)As structure by design because carriers in the semiconductor are not sufficiently magnetized at equilibrium due to the low Mn moment density and high temperature of the experiment. In principle, one might also consider that the spin-accumulation induced by the Dresselhaus ISGE could cause a diffusive spin-current to flow into the ferromagnet and exert an antidamping-like spin-transfer torque. This would have the Dresselhaus symmetry which is, however, not seen in our antidamping-like torque data.

A Rashba-symmetry antidamping-like SOT due to the carriers in the Fe experiencing the inversion-asymmetry of the interface could in principle also explain the symmetry of our data, however we do note the lack of a corresponding strong Rashba-symmetry field-like SOT. This antidamping SOT would have the same symmetry as the antidamping SHE-STT. This possibility is, however, ruled out by our control experiment in which we perform electrically detected FMR in a similar MBE-grown Fe (1 nm)/insulating GaAs structure at room temperature. In this case, we do not observe the anti-damping torque in the rectification effect, despite the sample possessing a similar magnetoresistance ratio ($\sim$0.2%) to our Fe/(Ga,Mn)As. This is consistent with the carriers being removed from the semiconductor which eliminates the SHE source of the spin-current. We note that also consistently with the absence of carriers in the semiconductor in the Fe/insulating-GaAs structure, we do not

observe the Dresselhaus-symmetry field-like SOT in this control sample.

Determining the magnitudes of the ISGE and SHE

To calibrate the microwave current in the sample we used a bolometric technique (see supplementary note 4). Using this calibration, we estimate amplitudes of $|\mu_0 h^{\mathrm{ISGE}}/J_{\mathrm{GaAs}}| = 16 \pm 10$ μT/10^6Acm^{-2} and $|\mu_0 h^{\mathrm{SHE}}/J_{\mathrm{GaAs}}| = 20 \pm 9$ μT/10^6Acm^{-2}. The error is found from the statistical variation of all of the devices measured. To verify the bolometric calibration, we also perform an additional check with a single device by measuring the change in Q-factor of the microstrip resonator loaded with and without a sample (see supplementary note 5). This calibration yields values of $|\mu_0 h^{\mathrm{ISGE}}/J_{\mathrm{GaAs}}| = 37$ μT/10^6Acm^{-2} and $|\mu_0 h^{\mathrm{SHE}}/J_{\mathrm{GaAs}}| = 47$ μT/10^6Acm^{-2}, close to the values of the bolometric technique.

From the measured h^{SHE} in our Fe/(Ga,Mn)As structure we can infer the room-temperature spin Hall angle, θ_{SH}, in the paramagnetic (Ga,Mn)As using the expression based on the antidamping-like STT[2],

$$\theta_{\mathrm{SH}} = \frac{2e}{\hbar}\mu_0 M_{\mathrm{s}} d_{\mathrm{Fe}} \frac{h^{\mathrm{SHE}}}{J_{\mathrm{GaAs}}}. \qquad (2)$$

Here it is assumed that the thickness of the semiconductor is much larger than its spin diffusion length (5.6 nm in p-GaAs[36]) and d_{Fe} is the thickness of the Fe layer. Eq. (2) yields values of $\theta_{\mathrm{SH}} = 1.7 \pm 0.9\%$ (bolometric calibration) and 4% (Q-factor calibration), similar to spin Hall angles previously reported for carriers with p-orbital character in GaAs[36,37]. This agreement with previously measured spin-Hall angles is further evidence that the antidamping-like torque does not have a significant Rashba-symmetry SOT contribution. To check these spin-Hall values we compare our torque efficiencies in terms of field per total current density with those of transition-metal/ferromagnet bilayers. For instance, Garello *et al.* measured an antidamping-like torque of $|\mu_0 h/J| = 690$ μT/10^6Acm^{-2} in layers with 0.6 nm Co and 3 nm Pt and an equivalent spin-Hall angle of 16%.[28] Although our spin-Hall angle is only 4-8 times smaller, the field per total current density is 85-170 times smaller because the total magnetic moment of our Fe layer is ~ 4 times higher than of the Co and $\sim 80\%$ of the total current is shunted through the Fe.

To conclude, we have experimentally disentangled the two archetype microscopic mechanisms that can drive relativistic current-induced torques in ferromagnet/paramagnet struc-

tures. In our epitaxial Fe/(Ga,Mn)As bilayer we simultaneously observed ISGE-based and SHE-based torques of comparable amplitudes. Designed magnetization-angle and current-angle symmetries of our single-crystal structure allowed us to split the two microscopic origins between the field-like and the antidamping-like torque components. Experimentally establishing the microscopic physics of the relativistic spin torques should stimulate both the fundamental and applied research of these intriguing and practical spintronic phenomena.

Methods

Thin-film growth

The semiconductor (Ga,Mn)As layer of thickness 20 nm was deposited on a GaAs(001) substrate by molecular beam epitaxy at a temperature of 260°C. The substrate temperature was then reduced to 0°C, before depositing a 2 nm Fe layer, plus a 2 nm Al capping layer. In-situ reflection high energy electron diffraction and ex-situ x-ray reflectivity and diffraction measurements confirmed that the layers are single-crystalline with sub-nm interface roughness.

Impedance matching

To improve the sensitivity of the FMR measurement, the sample is embedded in a microstrip resonator circuit[30] which acts to impedance match the $\sim$ 8 kΩ sample to the external 50 Ω transmission line at the fundamental frequency (in this case $\sim$ 8 GHz) or harmonic frequencies of the resonator (see supplementary note 1). To allow measurement of V_{dc}, the resonator contains an on-board bias-T. In this experiment, FMR measurements are made at the the 2$^{\mathrm{nd}}$ harmonic frequency of the resonator ($\sim$ 16 GHz).

Acknowledgements

The authors acknowledge support from EU European Research Council (ERC) advanced grant no. 268066, from the Ministry of Education of the Czech Republic grant no. LM2011026, from the Grant Agency of the Czech Republic grant no. 14-37427G and the Academy of Sciences of the Czech Republic Praemium Academiae. A.J.F. acknowledges support from a Hitachi research fellowship. H.K. acknowledges financial support from the Japan Science and Technology Agency (JST).

Author Contributions

K.O., R.P.C., B.L.G. and H.K. grew the materials. K.O. and H.K. prepared the samples. T.D.S., L.K.C. and H.K. performed the experiments and T.D.S. analysed the data. T.D.S., T.J. and A.J.F. prepared the manuscript. T.D.S. and A.J.F. planned the project.

REFERENCES

[1] Miron, I. M. *et al.* Perpendicular switching of a single ferromagnetic layer induced by in-plane current injection. *Nature* **476**, 189–193 (2011).

[2] Liu, L. *et al.* Spin-torque switching with the giant spin hall effect of tantalum. *Science* **336**, 555–558 (2012).

[3] Jungwirth, T., Wunderlich, J. & Olejník, K. Spin hall effect devices. *Nature mater.* **11**, 382–390 (2012).

[4] Ralph, D. & Stiles, M. D. Spin transfer torques. *J. Magn. Magn. Mater.* **320**, 1190–1216 (2008).

[5] Ivchenko, E. & Ganichev, S. Spin-photogalvanics. In *Spin Physics in Semiconductors*, 245–277 (Springer, 2008).

[6] Bernevig, B. A. & Vafek, O. Piezo-magnetoelectric effects in p-doped semiconductors. *Phys. Rev. B* **72**, 033203 (2005).

[7] Manchon, A. & Zhang, S. Theory of nonequilibrium intrinsic spin torque in a single nanomagnet. *Phys. Rev. B* **78**, 212405 (2008).

[8] Chernyshov, A. *et al.* Evidence for reversible control of magnetization in a ferromagnetic material by means of spin-orbit magnetic field. *Nature Phys.* **5**, 656–659 (2009).

[9] Kato, Y. K., Myers, R. C., Gossard, A. C. & Awschalom, D. D. Observation of the spin Hall effect in semiconductors. *Science* **306**, 1910–1913 (2004).

[10] Kato, Y., Myers, R. C., Gossard, A. C. & Awschalom, D. D. Current induced electron spin polarization in strained semiconductors. *Phys. Rev. Lett.* **93**, 176601 (2004). arXiv:cond-mat/0403407.

[11] Wunderlich, J., Kaestner, B., Sinova, J. & Jungwirth, T. Experimental observation of the spin Hall effect in a two dimensional spin-orbit coupled semiconductor system. *Phys. Rev. Lett.* **94**, 047204 (2005). arXiv:cond-mat/0410295.

[12]Aronov, A. G. & Lyanda-Geller, Y. B. Nuclear electric resonance and orientation of carrier spins by an electric field. *JETP Lett.* **50**, 431 (1989).

[13]Edelstein, V. M. Spin polarization of conduction electrons induced by electric current in two-dimensional asymmetric electron systems. *Solid State Commun.* **73**, 233–235 (1990).

[14]Mal'shukov, A. G. & Chao, K. A. Optoelectric spin injection in semiconductor heterostructures without a ferromagnet. *Phys. Rev.* **B 65**, 241308 (2002).

[15]Silov, A. Y. *et al.* Current-induced spin polarization at a single heterojunction. *Appl. Phys. Lett.* **85**, 5929–5931 (2004).

[16]Ganichev, S. D. *et al.* Can an electric current orient spins in quantum wells (2004). arXiv:cond-mat/0403641.

[17]Endo, M., Matsukura, F. & Ohno, H. Current induced effective magnetic field and magnetization reversal in uniaxial anisotropy (Ga,Mn)As. *Appl. Phys. Lett.* **97**, 222501–222501 (2010).

[18]Fang, D. *et al.* Spin-orbit driven ferromagnetic resonance: A nanoscale magnetic characterisation technique. *Nature Nanotech.* **6**, 413–417 (2011). arXiv:1012.2397.

[19]Miron, I. M. *et al.* Current-driven spin torque induced by the Rashba effect in a ferromagnetic metal layer. *Nature Mater.* **9**, 230–234 (2010).

[20]Pi, U. H. *et al.* Tilting of the spin orientation induced by Rashba effect in ferromagnetic metal layer. *Appl. Phys. Lett.* **97**, 162507 (2010).

[21]Suzuki, T. *et al.* Current-induced effective field in perpendicularly magnetized Ta/CoFeB/MgO wire. *Appl. Phys. Lett.* **98**, 142505 (2011).

[22]Pesin, D. A. & MacDonald, A. H. Quantum kinetic theory of current-induced torques in rashba ferromagnets. *Phys. Rev.* **B 86**, 014416 (2012).

[23]Wang, X. & Manchon, A. Diffusive spin dynamics in ferromagnetic thin films with a Rashba interaction. *Phys. Rev. Lett.* **108**, 117201 (2012).

[24]Garate, I. & MacDonald, A. H. Influence of a transport current on magnetic anisotropy in gyrotropic ferromagnets. *Phys. Rev.* **B 80**, 134403 (2009). arXiv:0905.3856.

[25]Kurebayashi, H. *et al.* An anti-damping spin-orbit torque originating from the berry curvature. *Nature Nanotech.* **9**, 211–217 (2014). arXiv:1306.1893.

[26]Freimuth, F., Blügel, S. & Mokrousov, Y. Spin-orbit torques in Pt/Co films from first principles (2013). arXiv:1305.4873.

[27]Pai, C. *et al.* Enhancement of perpendicular magnetic anisotropy and transmission of

spin-hall-effect-induced spin currents by a Hf spacer layer in W/Hf/CoFeB/MgO layer structures. *Appl. Phys. Lett.* **104**, 082407 (2014).

[28]Garello, K. *et al.* Symmetry and magnitude of spin-orbit torques in ferromagnetic heterostructures. *Nature Nanotech.* **8**, 587–593 (2013). arXiv:1301.3573.

[29]Kim, J. *et al.* Layer thickness dependence of the current-induced effective field vector in Ta—CoFeB—MgO. *Nature Mater.* **12**, 240–245 (2013).

[30]Fang, D. *et al.* Electrical excitation and detection of magnetic dynamics with impedance matching. *Appl. Phys. Lett.* **101**, 182402 (2012).

[31]Danan, H., Herr, A. & Meyer, A. J. P. New determinations of the saturation magnetization of nickel and iron. *J. Appl. Phys.* **39**, 669–670 (1968).

[32]Brockmann, M., Zolfl, M., Miethaner, S. & Bayreuther, G. In-plane volume and interface magnetic anisotropies in epitaxial Fe films on GaAs(001). *J. Magn. Magn. Mater.* **198-199**, 384–386 (1999).

[33]McGuire, T. & Potter, R. Anisotropic magnetoresistance in ferromagnetic 3d alloys. *IEEE Trans. Magn.* **11**, 1018–1038 (1975).

[34]Ando, K. *et al.* Angular dependence of inverse spin-Hall effect induced by spin pumping investigated in a NiFe/Pt thin film. *Phys. Rev. Lett.* **78**, 014413 (2008).

[35]Harder, M., Cao, Z. X., Gui, Y. S., Fan, X. L. & Hu, C. M. Analysis of the line shape of electrically detected ferromagnetic resonance. *Phys. Rev.* **B 84**, 054423 (2011).

[36]Chen, L., Matsukura, F. & Ohno, H. Direct-current voltages in (Ga,Mn)As structures induced by ferromagnetic resonance. *Nat. Commun.* **4**, 2055 (2013).

[37]Okamoto, N. *et al.* Electric control of the spin hall effect by intervalley transitions. *Nature Mater.* **13**, 932–937 (2014).

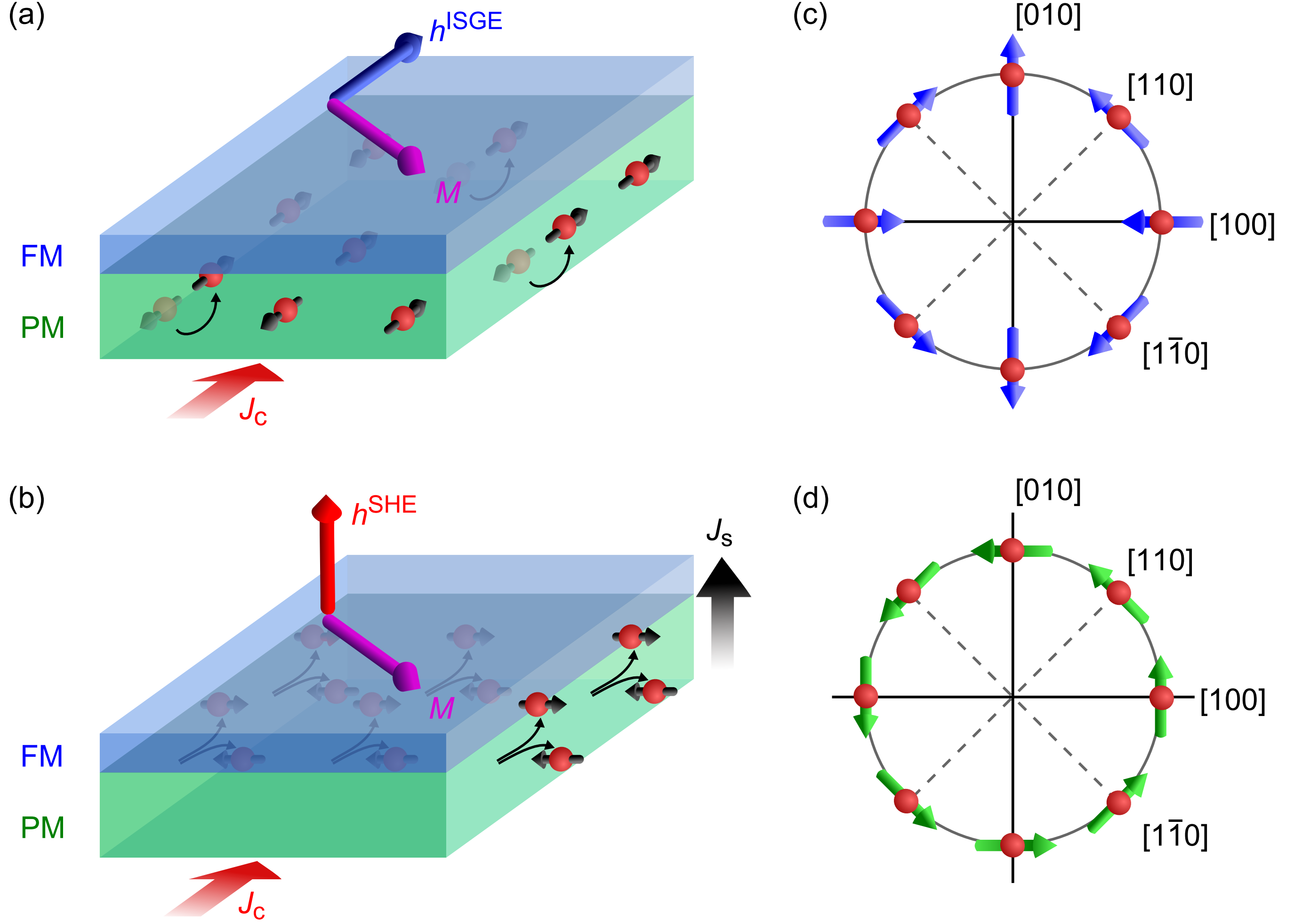

FIG. 1. **Microscopic origins of the SHE and ISGE torques** (a) In the paramagnetic GaAs layer (PM), as charge carriers are accelerated by an applied electric field in the inversion-asymmetric crystal potential, scattering events lead to a non-equilibrium spin-polarisation. The spin-polarisation depends on the direction of the current with respect to crystal direction. Through exchange coupling at the interface, the magnetisation, M, in the ferromagnetic layer (FM) experiences an effective field, h^{ISGE}, parallel to the spin-polarisation. (b) In the GaAs layer, when a longitudinal charge current, J_{c}, is applied, a transverse spin-current, J_{s}, is induced by the SHE, which flows into the Fe layer. The spin-current exerts a torque that depends on the magnetisation angle. For an in-plane magnetisation this is described by an out-of-plane effective field, h^{SHE}. (c) In GaAs, the spin-polarisation of the ISGE has the Dresselhaus symmetry for carrier momentum in different crystal directions. (d) This in contrast with transition metal bilayers where only the structural inversion-asymmetry may generate a spin-polarisation with Rashba symmetry.

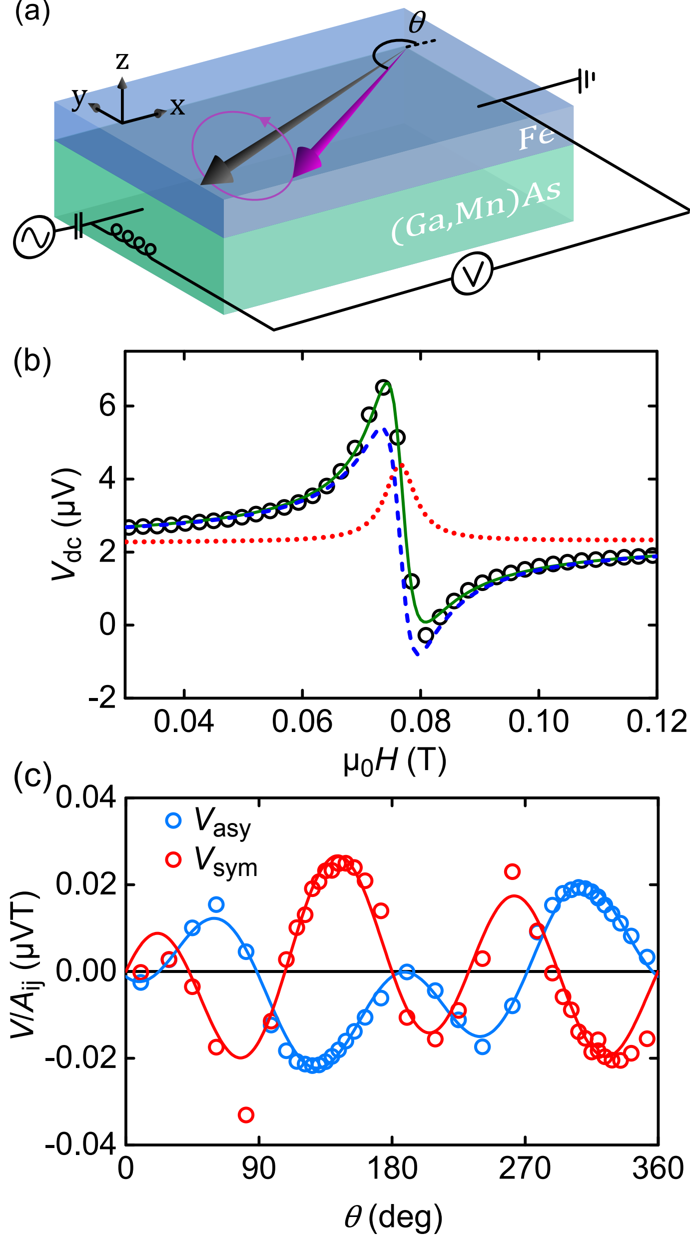

FIG. 2. **Electrical excitation and detection of FMR** (a) Schematic of the measurement showing magnetisation precession. A microwave current passes through the capacitor of the bias-T and into the Fe/GaAs bilayer sample where the current-induced torques causes the magnetisation of the Fe to precess around the external field. The precession is detected in the dc voltage measured across the device by a magnetoresistance mixing effect. (b) A typical SO-FMR curve detected in V_{dc} as a function of external field, induced by a 16.245 GHz microwave current. V_{dc} is fitted by a combination of symmetric (red dotted line) and antisymmetric (blue dashed line) Lorentzians. (c) The in-plane magnetisation angle dependence of the fitted Lorentzian amplitudes for a device with current in the [010] crystal direction. The full expression for the angle-dependence of the fitted data is given in the supplementary note 3.

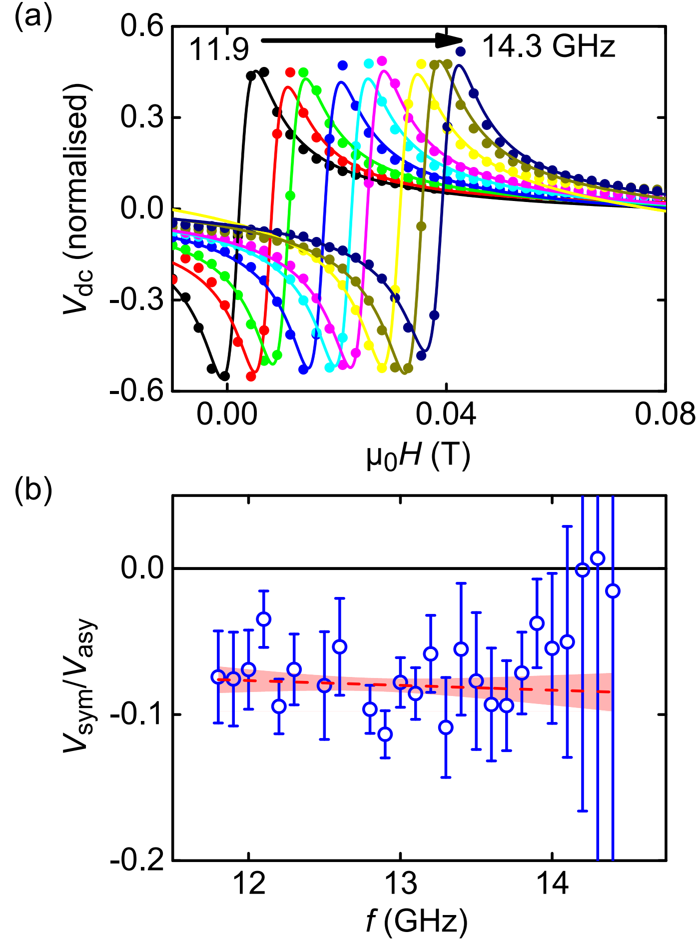

FIG. 3. **Frequency independence of the FMR lineshape** (a) Normalised, fitted, resonant peaks for a series of microwave frequencies detected in V_{dc}. The line-shape is dominated by an antisymmetric Lorentzian for every frequency. (b) The ratio of V_{sym} to V_{asy} (blue circles) is constant to within the the standard error of a linear fit (red dashed line) for the measured frequency range. The error in the ratio is bigger away from the impedance-matched frequency (13 GHz) of the microstrip resonator used as the detected peak in V_{dc} is smaller.

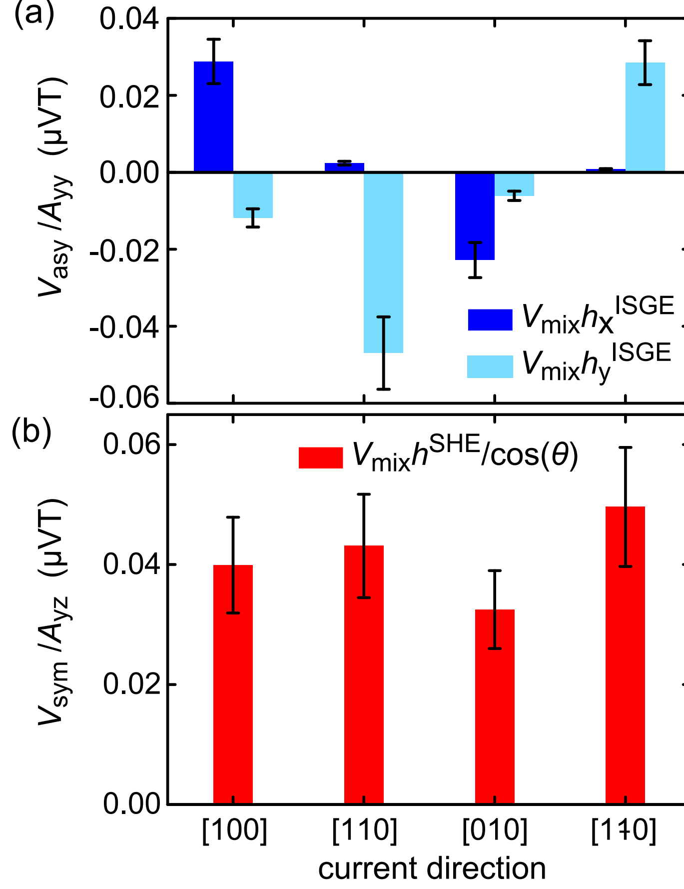

FIG. 4. **Dependence of the effective fields on the crystal direction of the current** (a) The fitted in-plane field coefficients for a set of devices in different crystal directions. (b) The fitted out of plane field coefficient (representing the antidamping torque) for the same devices. Error bars shown are calculated by estimating the error in V_{mix} due to the variance in the calibration of I_{mw}.